論文 / 著書情報
Article / Book Information

Title	Preparation of Soluble Polyimide/MgO Nanohybrid Films by In situ Hybridization Method and Evaluation of Their Thermal Conductivity
Authors	Kimiya MURAKAMI, Kazuhiko YAMADA, Kenzo DEGUCHI, Tadashi SHIMIZU, Shinji ANDO
Citation	Journal of Photopolymer Science and Technology, Vol. 23, No. 4, pp. 501-506
Pub. date	2010, 6

Journal of Photopolymer Science and Technology
Volume 23, Number 4 (2010) 501-506 ©2010CPST

Preparation of Soluble Polyimide/MgO Nanohybrid Films by *In situ* Hybridization Method and Evaluation of Their Thermal Conductivity

Kimiya MURAKAMI[1], **Kazuhiko YAMADA**[1], **Kenzo DEGUCHI**[2], **Tadashi SHIMIZU**[2], **and Shinji ANDO**[1]*

[1]*Department of Chemistry and Materials Science, Tokyo Institute of Technology, 2-12-1-E4-5 O-okayama, Meguro-ku, Tokyo 152-8552, Japan*
[2]*National Institute for Materials Science, 3-13 Sakura, Tsukuba, Ibaraki 305-0003, Japan*

For developing thermally stable polymer films exhibiting high thermal conductivity, fluorinated polyimides (PIs) were hybridized via '*in situ* hybridization method' and 'direct mixing method' with magnesium oxide (MgO) nanoparticles possessing high thermal conductivity and good insulating property. In the former method, MgO nanoparticles were spontaneously generated and precipitated in PI films by thermal decomposition of a soluble precursor, magnesium acetate tetrahydrate (MgAc). The Far-IR absorption spectra, WAXD patterns, and solid-state ^{25}Mg NMR spectra of PI/MgO hybrid films demonstrated that MgAc was thermally decomposed to MgO nanoparticles during curing up to 380 ^{o}C. In addition, the cross-sectional SEM images of the hybrid film showed that spherical MgO nanoparticles (average diameter : ~50 nm) were homogeneously dispersed without aggregation in the hybrid films. The thermal diffusivities along the out-of-direction ($\alpha_{\perp}$) of the hybrid films were measured using the temperature wave analysis, and their thermal conductivities (λ) were estimated from $\alpha_{\perp}$, specific heats, and densities. For the hybrid films prepared by both the methods, the λ values are proportionally increased as the MgO content increase, and the λ values are in good accord with the predicted values based on the Bruggeman's theory.

Keyword: soluble polyimide, hybrid, thermal diffusivity, MgO, *in situ* hybridization

1. Introduction

Recently, there has been a strong demand for thermally stable polymers having high thermal conductivity for electric, electronic, and photonic applications such as low-dielectric insulator films and passive/active layers for photonic devices. Hybridization of polymers with metal or inorganic nanoparticles has been widely used to improve their optical and thermal properties [1–6]. In this study, two hybridization methods were adopted. The first one is the 'direct mixing method' in which inorganic nanoparticles are directly mixed with a polymer matrix. Despite its simplicity, this method has a disadvantage that nanoparticles tend to aggregate due to their high surface energy. The second one is '*in situ* hybridization method' [7–9], in which nanoparticles are generated by the thermal decomposition of a soluble precursor. Although the thermal curing condition should be precisely controlled, this method has an advantage to preventing aggregation of nanoparticles.

Polyimides (PIs) are known to possess excellent physical properties and outstanding performance such as high thermal stability, and good mechanical, dielectric, and insulation properties [10]. However, conventional PIs have poor processability due to their insolubility and high glass-transition temperatures (T_gs). Thereby, PI films are generally prepared by the two-step procedure. Firstly, a solution of precursor of PI,

Received April 6, 2010
Accepted May 7, 2010

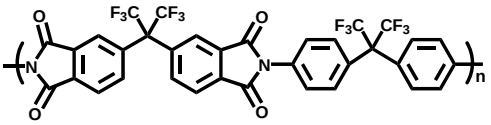

Scheme 1 Chemical structure of SIXEF-44

poly(amic acid) (PAA), is spin-coated onto a Si substrate. PAA has good processability due to the solubility in polar organic solvents. Secondly, the PAA film is thermally imidized at higher than 300°C. In contrast, soluble PIs have good processability even in the imidized (PI) state, and their T_gs are lower than those of conventional PIs, whereas soluble PIs possess excellent dielectric and optical properties. However, the thermal conductivities of any types of polymers are insufficient for future applications for dielectrics and substrates. Meanwhile, the thermal conductivity of magnesium oxide (MgO, 60 W/K·m) is two digits higher than those of conventional polymers (< 1 W/K·m). MgO can be prepared by the thermal decomposition of magnesium hydrate [11], magnesium acetate [11], magnesium alkoxide [12], and magnesium nitrate [13]. MgAc is stable in air, soluble in DMAc, and it shows a manageable decomposition temperature around 350 ºC. Hence, MgAc is suitable as a soluble precursor of MgO.

In this study, we attempted to enhance the thermal conductivities of soluble PI thin films by *in situ* hybridization with MgO nanoparticles. Soluble PI/MgAc hybrid films were formed on Si substrates, followed by thermal curing up to 380 ºC. The chemical compositions of PI/MgO hybrid films were analyzed by FT-IR, Far-IR, WAXD, and solid-state ^{25}Mg NMR. The thermal diffusivities along the out-of-direction of the hybrid film were measured by the temperature wave analysis [14], and the thermal conductivities were estimated from their thermal diffusivities, specific heats, and densities. Furthermore, the thermal conductivities of the hybrid films prepared by 'direct mixing method' and '*in situ* hybridization method' were compared with those predicted by the Bruggeman's theory.

2.Experimental

2.1. Materials

A soluble fluorinated polyimide (SIXEF-44, Scheme 1) obtained from Hoechst Celanese and magnesium acetate tetrahydrate ($Mg(CH_3COO)_2 \cdot 4H_2O$, MgAc) purchased from Kanto chemical Co., Inc were used as received. *N*,*N*-Dimethyl acetoamide (DMAc, anhydrous, 99.8%) purchased from Aldrich was dried with molecular sieves prior to use. Sub-μm size particles of MgO supplied by Ube Material Industries was used as received.

2.2. Preparation of PI/MgO hybrid films

2.2.1 *In situ* hybridization method

For preparing a DMAc solution of MgAc and PI (PI/MgAc solution), MgAc powder dried at 200 ºC for 1 h under reduced pressure was slowly added to a DMAc solution of SIXEF-44. PI/MgO hybrid films were prepared by spin-coating of PI /MgAc solution onto Si substrates, followed by drying at 70 ºC for 2 h under reduced pressure. The PI/MgO hybrid films were peeled from substrates and thermally cured at elevated temperatures up to 380 ºC under nitrogen flow. During thermal curing, MgAc dissolving in PI was expected to thermally decomposed to MgO. The films thus prepared are denoted as PI/MgO(i) films. The concentration of Mg atoms in PI/MgO hybrid films were set to 0–200 mol%.

2.2.2 Direct mixing method

To examine the enhancement of thermal conductivity in PI/MgO(i) films by hybridization with MgO, another type of PI/MgO hybrid films were prepared by 'direct mixing method'. MgO nanoparticles with average diameter of 200 nm were homogeneously dispersed in DMAc for 20 min by an ultrasonicator, and then powdery SIXEF-44 was added to dissolve in the solution. After stirring at room temperature for 12 h, PI/MgO hybrid films were prepared by spin-coating and thermal curing in the same procedure as PI/MgO(i) films. The films thus prepared are denoted as PI/MgO(d) films. The average thickness of all the samples was controlled as 15–20 μm via spin-coating rate in order to suppress the thickness dependence of experimental thermal diffusivity [15].

2.3. Measurements

The chemical composition of PI/MgO(i) films were analyzed by Fourier transform infrared (FT-IR) and FT-far-infrared (Far-IR) absorption spectra, wide angle X-ray diffraction (WAXD) patterns, and solid-state ^{25}Mg NMR. IR spectra were obtained with a Thermo-Nicolet AVATAR-320 FT-IR spectrometer, and Far-IR spectra were obtained with a JASCO FT/IR-6100 spectrometer. WAXD patterns were obtained with a Rigaku MiniFlex-II using operating at 35 kV and 15 mA with nickel-filtered Cu-Kα radiation. The scan was carried out in the 2θ range of 3° to 100°

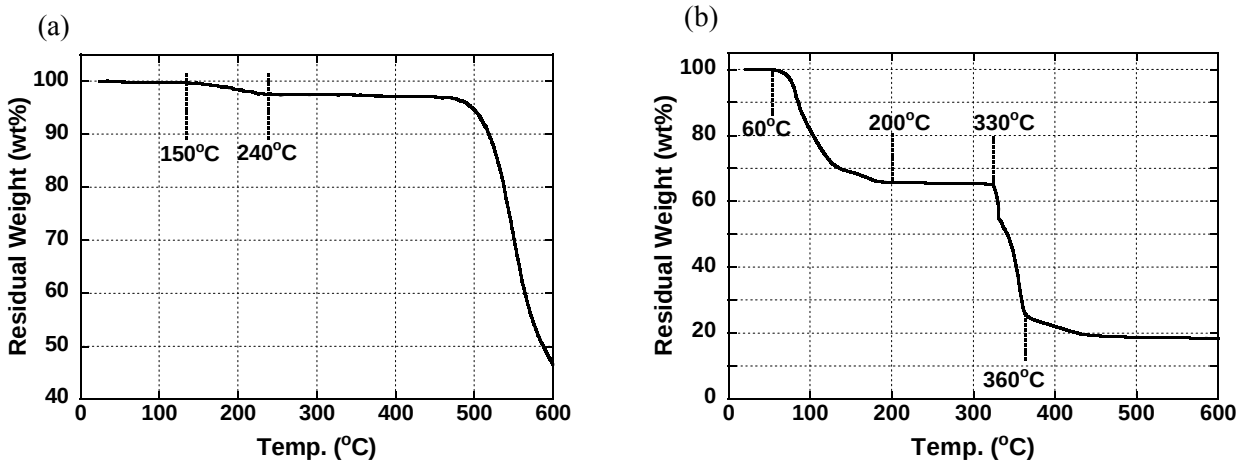

Fig.1 Thermolysis behavior of (a) SIXEF-44 and (b) MgAc tetrahydrate.

with an angle interval of 0.01° and a scan speed of 1°/min. Solid-state ^{25}Mg NMR experiments were performed on a JEOL ECA 930 spectrometer, operating at the frequency of 56.88 MHz at 21.82 T. MgO, MgAc, and PI/MgO(i) film were packed into ZrO_2 4-mm rotors. The spinning rate for ^{25}Mg MAS experiments was 16.0 kHz, and the recycle delay was set to be 3 s. Thermal diffusivity along the out-of-plane direction ($a_\perp$) and film thicknesses (d) of PI/MgO hybrid films were measured with a temperature wave analyzer (ai-Phase Mobile 1u). Thermal diffusivity was measured at three different points on sample films, and average value was taken as experimental $a_\perp$ value. The specific heat of a SIXEF-44 PI film was measured with a Shimadzu DSC-60 analyzer with a heating rate of 5 ºC/min under nitrogen [16]. The density of a PI film was measured by pycnometeric method using water as a medium. The thermolysis (thermal decomposition) behaviors of PI films and MgAc powder were recorded with a Shimadzu TG/DTA-60 analyzer in the temperature range between room temperature and 900 ºC at a heating rate of 5 ºC/min under nitrogen. The cross-sectional images of pristine PI and PI/MgO hybrid films were observed with a scanning electron microscope (Hitachi, S-4500). Sample films formed on Si substrates were fractured by the freeze-fracture method using liquid nitrogen.

3. Results and Discussion

3.1. Thermolysis behaviors of PI and MgAc

The thermolysis behaviors (TGA curves) of SIXEF-44 and MgAc are shown in Fig. 1. As seen in Fig. 1(a), the 5 wt% decomposition temperature (T_d^5) of SIXEF-44 (510 ºC) is much higher than the curing temperature (380 ºC) of PI/MgO hybrid films. The decrease in weight between 150 ºC and 240 ºC is attributable to the dehydration caused by

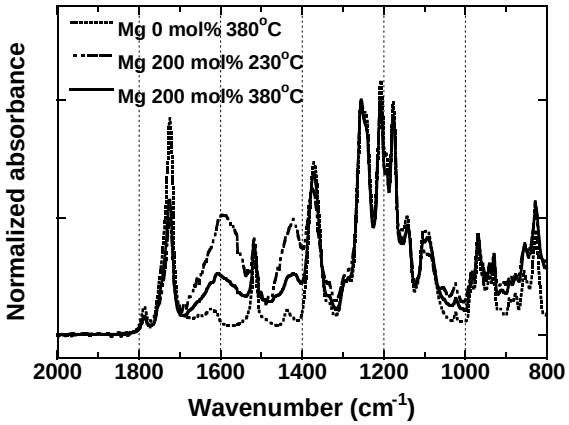

Fig.2 IR spectra of hybrid films prepared with different heat treatment temperature.

imidization of residual amide acid. A significant amount of amide acid was remained in the as-received SIXEF-44 to afford solubility to solvents. The degree of imidization of the PI was estimated as 45.4 mol%. In addition, as shown in Fig. 1(b), the thermal degradation of MgAc was proceeded in two steps. The first step between 60 ºC and 200 ºC represents the desorption of crystal water, in which MgAc was transformed from tetrahydrate to anhydrate. The second step between 330 ºC and 360 ºC with a rapid decrease in weight was attributable to the thermal decomposition of MgAc, which generates MgO [17]. Hence, the thermal treatment of PI/MgAc films up to 380 ºC induced completion of imidization of SIXEF-44 and decomposition of MgAc followed by generation of MgO without deterioration of PI matrix.

3.2. Chemical composition of PI/MgO(i) films

The chemical composition of the PI/MgO(i) films thus prepared were analyzed by IR, Far-IR, and WAXD. Fig. 2 shows the IR spectra of the hybrid films cured at two different temperatures, 230 ºC and 380 ºC. The peak intensities were normalized using the absorption band at 1255 cm^{-1}

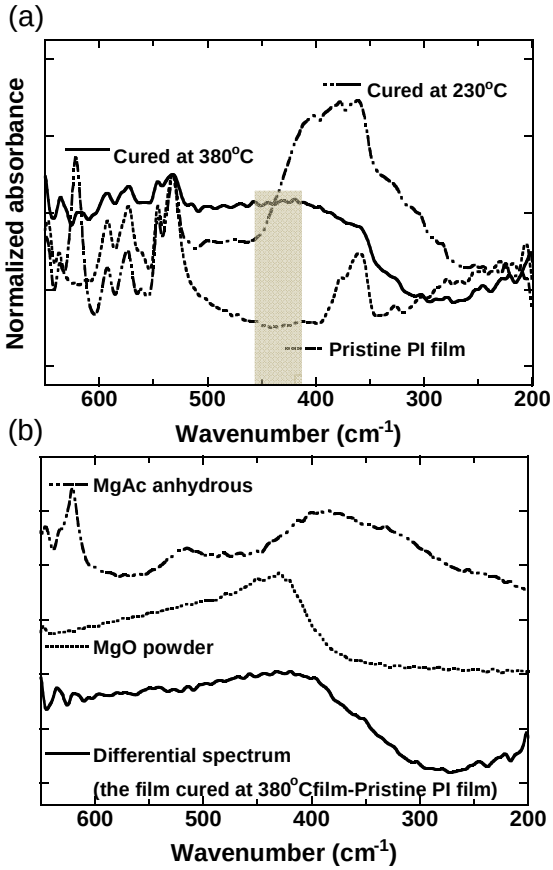

Fig.3 (a) Effect of heat treatment temperature on Far-IR spectra.(b)Comparison of the far-IR spectra of MgAc and MgO with the differential spectrum calculated using the spectra of the film cured at 380°C and pristine PI.

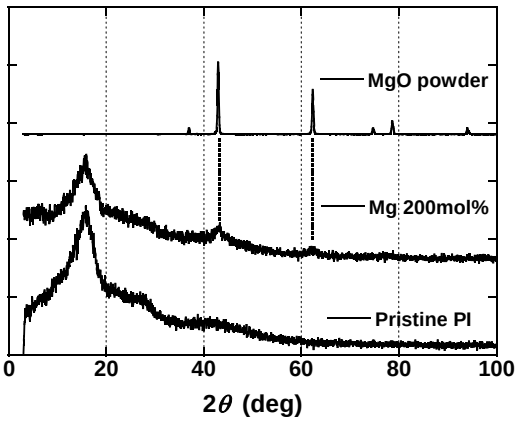

Fig.4 WAXD patterns of PI/MgO(i) films and MgO powder.

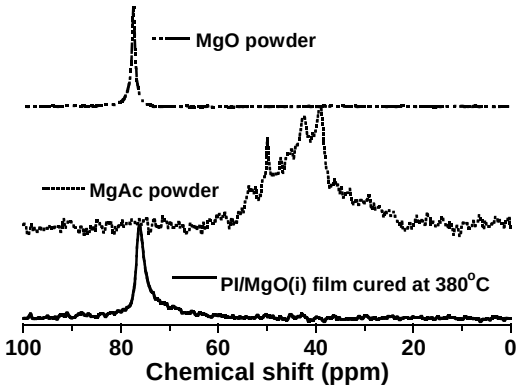

Fig.5 Solid-state ^{25}Mg NMR spectra of MgO and MgAc powders and PI/MgO(i) film cured at 380°C.

which is assignable to C–F stretch of SIXEF-44. Compared with the film cured at 230 ºC (230 ºC film), the film cured at 380 ºC (380 ºC film) shows two weak bands assignable to MgAc (1437 and 1600 cm^{-1}). These are attributable to the symmetric and anti-symmetric stretchings of carboxylate ion, respectively. These facts indicate that MgAc was decomposed to MgO even in the PI hybrid films by thermal curing up to 380 ºC.

Fig. 3(a) shows the Far-IR spectra of PI/ MgAc films (Mg : 200 mol%) cured at 230 °C and 380 °C together with that of pristine PI (Mg : 0 %). The peak intensities were normalized using the band at 532 cm^{-1} which is assignable to the PI main chain. The spectrum of 230 °C film shows a strong and wide absorption band around 350–410 cm^{-1} which is attributable to MgAc. In contrast, the Far-IR spectrum of 380 °C film shows a very broad band at a center of 430 cm^{-1} with a weak shoulder around 400 cm^{-1}. The absence of the MgAc band indicates the decomposition of MgAc after 380 °C treatment. Since these bands are not observed in the spectrum of pristine PI, the absorptions in the difference spectrum should be attributed to decomposed components of MgAc. Thereby, the band around 430 cm^{-1} is assignable to MgO.

Fig. 3(b) shows the Far-IR spectra of dried MgAc powder, MgO powder, and the difference spectrum between 380 °C film and pristine PI film. The wide absorption at 350–410 cm^{-1} of MgAc coincides well that observed for PI/MgAc hybrid films cured at 230 °C (Fig. 3(a)) In contrast, both the MgO spectrum and the difference spectrum show a broad peak around 430 cm^{-1} with a weak shoulder extending to 400−350 cm^{-1}. In addition, these spectral shapes are entirely different from that of MgAc.

Fig. 4 shows the WAXD patterns of MgO powder, PI/MgO(i) hybrid, and the pristine PI films. The films containing 200 mol% of Mg show two peaks attributable to the crystalline MgO, which are absent in the pristine PI film. These facts indicate that MgO nanoparticles generated in PI/MgO(i) films was partly crystallized, which gave the characteristic MgO diffractions.

Fig. 5 shows experimental ^{25}Mg MAS spectra

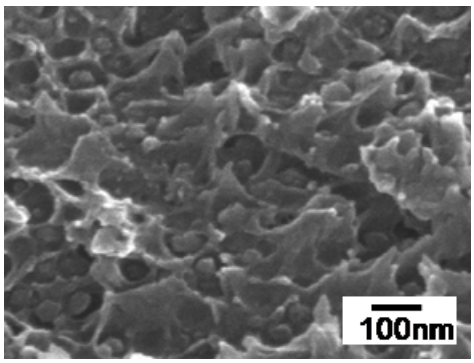

Fig.6 Cross-sectional SEM image of PI/MgO(i) film.

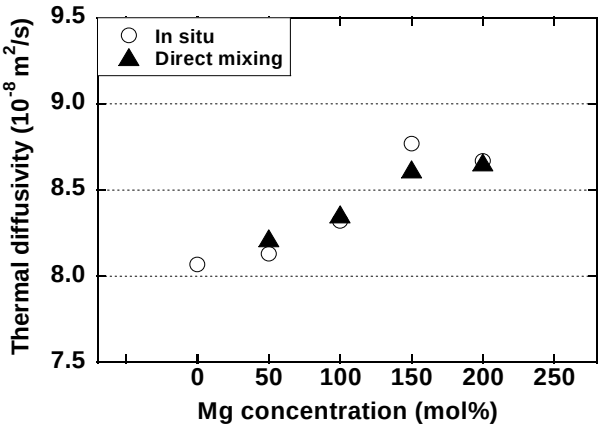

Fig.7 Measured thermal diffusivities of PI/MgO(i) and PI/MgO(d) films containing different MgO concentration.

of MgO and MgAc powders, and PI/MgO(i) film cured at 380°C. The NMR spectrum of PI/MgO(i) film coincides well with that of MgO, but far different from that of MgAc. In consequence, these facts support that MgAc was converted to MgO within PI/MgO(i) films during thermal curing.

Fig. 6 shows the cross-sectional SEM images of PI/MgO(i) films cured at 380 °C. Note that the generated MgO nanoparticles having spherical shapes (average diameter : 50 nm) are homogeneously dispersed in the films, and the nanoparticles are well covered and encapsulated with matrix PI. The absence of aggregated structures of MgO nanoparticles strongly supports the advantage of '*in situ* hybridization method'.

3.3. Thermal conductivity of PI/MgO hybrid films

Fig. 7 shows the experimental thermal diffusivities ($a_\perp$) of PI/MgO(i) films prepared with different MgO concentrations. The MgO concentrations of PI/MgO(i) films were calculated under an assumption that MgAc dissolved in hybrid films was completely decomposed to MgO. A nearly linear relationship between the MgO contents in the PI/MgO(i) films and the $a_\perp$ values

Table.1 Thermal conductivities of hybrid films. (W/K·m)

MgO content (mol %)	PI/MgO(i) films	PIMgO(d) films	Calculated
0	0.138	0.138	0.138
50	0.142	0.140	0.143
100	0.146	0.145	0.148
150	0.152	0.155	0.153
200	0.154	0.155	0.158

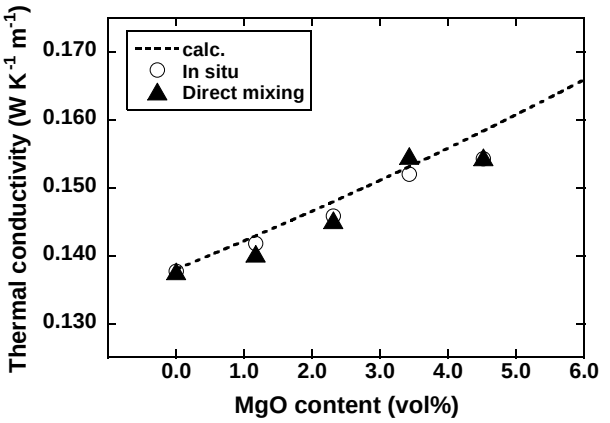

Fig.8 Measured and calculated thermal conductivities of PI/MgO(i) films and PI/MgO(d) films.

is observed, which indicates that '*in situ* hybridization method' is a facile and powerful technique to enhance the thermal diffusivity of PI films with precise controllability of nanoparticles.

In general, thermal conductivity (λ) is widely used as a measure for heat transfer of materials compared with thermal diffusivity ($a_\perp$). λ can be estimated using the following eqs. (1)−(3):

$$\lambda = \alpha C_p \rho \quad (1)$$

$$C_{ph} = C_{pm}\phi + C_{pp}(1-\phi) \quad (2)$$

$$\rho_h = \rho_m\phi + \rho_m(1-\phi) \quad (3)$$

where C_p is the specific heat of a material, ρ the density, and ϕ the volume fraction of nanoparticles (MgO). The subscripts *h*, *p*, and *m* represent hybrid sample, matrix polymer, and dispersed MgO, respectively. The values of C_p and ρ of hybrid films (C_{ph} and ρ_h) were calculated from the literature data for MgO (C_{pm}=924 (J/K kg), and ρ_m =3.58 (g/cm^3)) [18, 19] and the experimental data for PI (C_{pp}=1.066 (J/K kg), ρ_p =1.60 (g/cm^3)).

Fig. 8 shows the experimental thermal conductivities (λ_h) of PI/MgO(i) and PI/MgO(d) films cured at 380 °C, in which the contents of MgO are indicated by vol%. The solid line in Fig. 8 represents the theoretical thermal conductivities (λ_h^{cal}) of PI/MgO hybrid films estimated based on the Bruggeman's theory [20]. (eq. (4)):

$$1-\phi=\frac{\lambda_m-\lambda_h}{\lambda_m-\lambda_p}\left(\frac{\lambda_p}{\lambda_h}\right)^{\frac{1}{3}} \qquad (4)$$

The λ value of MgO was taken from the literature (λ_d=60 (W/K·m)) [21], and the calculated λ_h^{cal} values are also listed in Table 1. Note that the experimental λ_h values of PI/MgO(i) shows a linear relationship with the incorporated MgO content, and the λ_h values agree well with the calculated λ_h^{cal} values. This should be related to the homogeneous dispersion of MgO nanopaticles even at a high MgO content with lesser thermal resistance at boundaries between PI and MgO. In addition, it was also shown that the Bruggeman's theory is a useful tool to predict the λ_h values of inorganic/organic hybrid systems [22, 23].

It should be noted that the experimental λ_h values of PI/MgO(d) films, in which spherical sub-μm (~0.2 μm) MgO particles are dispersed by direct mixing, are also close to those of PI/MgO(i) films as well as the calculated λ_h^{cal}. The fact that the λ_h of PI/MgO(i) films are comparable to those of PI/MgO(d) films indicates that the size of MgO nanoparticle does not lead to significant difference in thermal conductivity of PI/MgO hybrids.

4. Conclusion

PI/MgO nanohybrid films were successfully prepared by '*in situ* hybridization method' using a mixture of a soluble fluorinated PI (SIXEF-44) and a soluble precursor of MgO (MgAc). The TGA curve of PI/MgAc films demonstrated that the thermal treatment at 380 ºC induced decomposition of MgAc to MgO without degradation of PI matrix. The spectroscopic characterization of PI/MgO hybrid films indicated that most of MgAc was thermally decomposed to MgO, and the MgO nanoparticles were partly crystallized in PI/MgO(i) films. The cross-sectional SEM image of PI/MgO(i) films showed that MgO nanoparticles with average diameter of 50 nm were homogeneously dispersed in the films without aggregation.

The thermal diffusivity of PI/MgO(i) films ($a_\perp$) is linearly proportional to the MgO content up to 200 mol%, which indicates that the homogeneous dispersion of MgO nanoparticles effectively enhances the $a_\perp$ of PI films. The thermal conductivities (λ_h) of PI/MgO(i) and PI/MgO(d) films, estimated from $a_\perp$, C_p, and ρ, are close to each other at all the MgO contents, and these values are agree well with the calculated λ_h^{cal} values based on the Bruggeman's theory. In summary, the PI/MgO hybrid material prepared by '*in situ* hybridization method' and 'direct mixing method' exhibit high thermal conductivity with maintaining the inherent properties of pristine PI. In particular, '*in situ* hybridization' with MgO is a facile and effective way to prepare thermally stable and thermally conductive PI films for a wide range of applications.

References

1. D. Yorifuji, A. Matsumura, T. Aoki, Y. Tashiro, S. Kuroki and S. Ando, *J. Photopolym. Sci. Technol.*, **22**, (2009) 447.
2. Y. Watanabe, Y. Sakai, Y. Shibasaki, S. Ando and M. Ueda, *Macromolecules*, **35** (2002) 2277.
3. S. Matsuda, Y. Yasuda, and S. Ando, *Adv. Mater.*, **17**, (2005) 2221.
4. S. Ando, *SPIE Photonics West '09 (San Jose, USA, Jan'09)*, **7213**, (2009) 72130B-1-10.
5. Y. P. Mamunya, V. V. Davydenko, P. Pissis, and E. V. Lebedev, Euro. *Polym. J.*, **38**, (2002) 1887.
6. R. Haggenmueller, C. Guthy, J. R. Lukes, J. E. Fischer, and K. I. Winey, *Macromolecules*, **40**, (2007) 2417.
7. T. Sawada, and S. Ando, *Chem. Mater.*, **10**, (1998) 3368.
8. S. Matsuda, and S. Ando, *Jpn. J. Appl. Phys.*, **44**, (2005) 187.
9. A. Somwangtanaroj, A. Matsumura, and S. Ando, *Proc. SPIE*, **6122**, (2006) 58.
10. S. Ando, *J. Photopolym. Sci. Technol.*, **17** (2004) 219.
11. E. M. van der Merwe and C. A. Strydom, *J. Therm. Anal. Cal.*, **76**, (2004) 149.
12. H. S. Jung, J. K. Lee,1 J. Y. Kim, and K. S. Hong, *J. Colloid Interface Sci.* **259** (2003) 127.
13. F. Paulik, J. Paulik, M. Arnold, and R. Nauman, *J. Therm. Anal.* **34**, (1988), 627.
14. J. Morikawa and T. Hashimoto, *J. Therm. Anal. Cal.*, **64**, (2001) 403.
15. F. Takahashi, K. Ito, J. Morikawa, T. Hashimoto, and I. Hatta, *Jpn. J. Appl. Phys.*, **43**, (2004) 7200.
16. J. Fujino, and T. Honda, *Netsu Bussei*, **20**, (2006) 166.
17. S. C. Mojumdar, E.Jona, and M.Melnik, *J. Therm. Anal. Cal.*, **60**, (2000) 571.
18. *J. Phys. Chem. Ref. Data,* **14**, Supl.1, (1985) 1469.
19. R. Kubo, S. Nagakura, H.Inokuchi, and H. Ezawa, eds., *Iwanami Rikagaku Jiten* [*Iwanami physics and chemistry dictionary*] 4th edition (1987) 502, Iwanami, Tokyo.
20. D.A.G. Bruggeman, *Ann. Phys.*, **24**, (1935) 636.
21. *Kagaku Binran Kisohen* [*The Chemistry Handbok basic edition*] ed. the Chemical Society of Japan, 5th edition, 2-74 (2004) Maruzen, Tokyo.
22. E. Yamada, *Netsu Bussei*, **3**, (1989) 78.
23. K.Kanari, and T. Ozawa, *Netsu Bussei*, **3**, (1989) 106